

Empirical Investigation on the Impact of Hydrogen Collisions for the Formation of C I 1.07 μm Lines Based on the Solar Center-to-Limb Variation *

Yoichi TAKEDA

National Astronomical Observatory, 2-21-1 Osawa, Mitaka, Tokyo 181-8588

takeda.yoichi@nao.ac.jp

and

Satoru UENO

Kwasan and Hida Observatories, Kyoto University,

Kurabashira, Kamitakara, Takayama, Gifu 506-1314

ueno@kwasan.kyoto-u.ac.jp

(Received 2013 September 19; accepted 2013 October 30)

Abstract

With an aim of examining the validity of non-LTE line-formation calculations for the strong C I lines of multiplet 1 at 1.068–1.069 μm , especially in terms of the treatment of collisions with neutral hydrogen (H I) atoms, we computed theoretical equivalent widths (W_λ) of these lines corresponding to specific intensities of different angles ($\mu = \cos\theta$) on the solar disk under various conditions, which were then compared with the empirical W_λ vs. μ relations obtained from our spectroscopic observations using the Domeless Solar Telescope at Hida Observatory. It turned out that our observational data are almost consistent with the theoretical simulations done with the H I collision rates computed with the classical formula, which suggests that the necessity of its significant revision (e.g., considerable reduction) is unlikely.

Key words: Atomic data — line: formation — Sun: abundances — Sun: atmospheres

1. Introduction

Recently, Takeda and Takada-Hidai (2013, hereinafter referred to as TTH13) showed that a group of strong C I lines at $\sim 1.07 \mu\text{m}$ in the near-IR region (multiplet 1; $3s\ ^3\text{P}^\circ - 3p\ ^3\text{D}$; $\chi_{\text{low}} \sim 7.5 \text{ eV}$) are quite useful for investigating the carbon abundances of old metal-deficient

* Based on data collected by the Domeless Solar Telescope at Hida Observatory (Kyoto University, Japan).

stars, thanks to their visibility down to the extremely metal-poor regime irrespective of the type of stars. For example, these C I lines are applicable not only to metal-poor giants (of lower T_{eff} and lower $\log g$) but also to very metal-poor turn-off stars (of higher T_{eff} and higher $\log g$), for which CH molecular lines (widely used for C abundance determinations of population II stars) become too weak to be measurable due to their large sensitivity to T_{eff} . Besides, these near-IR lines in the J -band are superior to other occasionally-used C I lines of multiplet 3 at $0.91 \mu\text{m}$, because of being unaffected by telluric lines.

As TTH13 pointed out, however, these strong near-IR lines suffer considerably large non-LTE effects ($|\Delta| \sim 0.1\text{--}0.5$ dex; where Δ is the negative non-LTE abundance correction; cf. figure 4b in TTH13), the extents of which tend to progressively increase with a decrease in metallicity. Moreover, these corrections were found to be sensitive to how the collisional rates due to neutral hydrogen atoms are included; i.e., while TTH13 adopted the practical formula derived by Steenbock and Holweger (1984) based on Drawin's (1968, 1969) classical cross sections for evaluating these H I collisions, $|\Delta|$ would become even doubled if these classical rates are reduced by a factor of 10 (cf. figure 4c in TTH13). This problem has a significant impact in connection with the systematic discrepancy between the abundances derived from these C I lines and CH molecular lines, as discussed in TTH13. It is thus important to check whether or not the classical treatment for these H I collisions is reasonable in an empirical manner.

Given this situation, we decided to make use of the center-to-limb variation of the strengths of these lines on the solar disk, as suggested by TTH13, with an intention to provide some empirical constraint on this issue by comparing the theoretical results (calculated under various conditions) with the new observational data obtained by ourselves. The purpose of this paper is report on this investigation.

The remainder of this article is organized as follows. After describing our solar observations and measurements of equivalent widths in section 2, we explain theoretical calculations of equivalent widths along with the adopted solar model atmospheres in section 3. Section 4 is devoted to discussing the characteristics of theoretically computed results, which are further compared with the observational data to reach a conclusion. Besides, we briefly mention the results for the O I 7771–5 Å triplet lines (also targeted in our observations) in appendix 1, followed by appendix 2 where the temperature structure of the solar photospheric model adopted in this study is compared with those of various other models.

2. Observations and Measurements

2.1. Observational Data

The observations were carried out on 2013 July 26 (JST)¹ by using the 60 cm Domeless Solar Telescope (DST) with the Horizontal Spectrograph of the Hida Observatory, Kyoto University (Nakai & Hattori 1985). Regarding the target positions on the solar disk, we selected 12 points on the meridian line of the solar disk (1 point at the disk center and 11 points from $0.45 R_0$ to $0.95 R_0$ with a step of $0.05 R_0$), at which the slit was aligned in the E–W direction on the Sun as depicted in figure 1. In the adopted setting of the spectrograph, our observation produced a solar spectrum with a resolving power of $R \sim 190,000^2$ covering $145''$ (spacial) and $10680\text{--}10697 \text{ \AA}$ (wavelength) on the CCD detector (800 pixels in the dispersion direction and 600 pixels vertical to the dispersion direction). The data reduction was done by following the standard procedures (dark subtraction, flat-fielding, spectrum extraction, wavelength calibration, continuum normalization), where the final 1D spectrum was extracted by integrating over 166 pixels ($= 40''$; i.e., ± 83 pixels centered on the target point) in the direction of the slit. Although some interference fringes could not be completely removed, we could attain S/N ratios on the order of $\sim 100\text{--}150$, which are sufficient for measuring equivalent-widths.

The resulting spectra are displayed in figure 2 (disk center spectrum) and figure 3 (12 spectra at different μ^3), where the reference disk-center spectrum ($R \sim 350,000$) of the same region taken from the published solar FTS spectrum atlas⁴ (Neckel 1994, 1999) is also shown for comparison. As can be recognized from figure 2, the lines in our disk-center spectrum (red symbols) are generally shallower than the reference FTS spectrum (blue lines). This indicates that our spectra are influenced by appreciable scattered light, which must be corrected as will be described in subsection 2.3.

2.2. Evaluation of Equivalent Widths

As to evaluating the equivalent widths of three C I lines at 10683.08 , 10685.34 , and 10691.24 \AA , attention should be paid to realizing sufficiently high internal accuracies between

¹ The aspect angles of the solar rotation axis (P : position angle between the geographic north pole and the solar rotational north pole; B_0 : heliographic latitude of the central point of the solar disk) on this date were ($+8^\circ 22'$, $5^\circ 19'$).

² The entrance slit (0.05 mm width) projects a shadow corresponding to 0.0288 \AA width on the detector while the theoretical resolution of the grating is 0.0468 \AA . The root-sum-square of these two makes a wavelength resolution of 0.055 \AA (corresponding to ~ 2.5 pixels). Consequently, the resolving power is $R \simeq 10690/0.055 \sim 190,000$.

³ As usual, μ is the direction cosine defined as $\cos\theta$, where θ is the angle between the line of sight and the normal to the surface at the observing point.

⁴ This spectrum atlas, which is based on disk-center observations of the Sun by using the Fourier Transform Spectrometer at the McMath telescope of the National Solar Observatories at Kitt Peak, is available at (<ftp.hs.uni-hamburg.de/pub/outgoing/FTS-Atlas>).

the spectra of different μ values. Given that some lines are partially blended with each other (e.g., Si I 10689.72 and C I 10691.12) and these C I lines show appreciable damping wings, we considered that the conventional approach (e.g., direct measurement or Gaussian fitting) is not appropriate in the present case.

Therefore, we adopted an alternative approach applied by TTH13 (cf. subsections 3.2 and 3.3 therein) based on a spectrum-synthesis modeling. That is, we first fitted the theoretical synthetic spectrum $[I^{\text{th}}(\lambda, \mu)$; computed for a given model atmosphere] with the observed spectrum $[I^{\text{obs}}(\lambda, \mu)]$ by finding the most optimal solutions of $\log \epsilon(\text{C})$ and $\log \epsilon(\text{Si})$ (C and Si abundances), where the automatic fitting algorithm (Takeda 1995a) was applied for this purpose. The finally accomplished fit for each spectrum is shown in figure 3. Then, the equivalent widths (W_λ) of three C I lines were *inversely* computed from such established solution of $\log \epsilon(\text{C})$ by using the same model atmosphere.⁵

2.3. Scattered-Light Correction

The apparent W_λ values derived in the previous subsection need to be corrected for scattered light. In order to tackle this problem, we postulate two assumptions in analogy with the procedure adopted by Allende Prieto et al. (2004) and Pereira et al. (2009a):

- (i) The scattered light occurs inside the spectrograph, which is wavelength-independent (i.e., not dispersed into spectrum) and proportional to the incident radiation (i.e., continuum intensity) coming through the slit.
- (ii) The reference disk-center spectrum of solar FTS spectrum atlas (Neckel 1994, 1999) is not affected by any scattered light.

From assumption (i), we can write the scattered light I_{scat} as a fraction α of the continuum intensity I_{cont} ($I_{\text{scat}} = \alpha I_{\text{cont}}$). Then, the “true” line depth $R(\lambda)$ and the “apparent” line depth $R'(\lambda)$ are expressed as follows:

$$R(\lambda) \equiv 1 - \frac{I(\lambda)}{I_{\text{cont}}}, \quad (1)$$

$$R'(\lambda) \equiv 1 - \frac{I(\lambda) + I_{\text{scat}}}{I_{\text{cont}} + I_{\text{scat}}} = 1 - \frac{I(\lambda) + \alpha I_{\text{cont}}}{I_{\text{cont}} + \alpha I_{\text{cont}}} = \frac{1}{1 + \alpha} \left(1 - \frac{I(\lambda)}{I_{\text{cont}}} \right). \quad (2)$$

Since the true and apparent equivalent widths are defined as $W_\lambda \equiv \int R(\lambda) d\lambda$ and $W'_\lambda \equiv \int R'(\lambda) d\lambda$, respectively, equations (1) and (2) lead to the following relation:

$$W'_\lambda = W_\lambda / (1 + \alpha). \quad (3)$$

⁵ For example, in the case of the C I 10683.08 line, the equivalent width (W'_{10683}) was computed by using Kurucz’s (1993) WIDTH9 program (curve-of-growth mode) from (1) the solution of $\log \epsilon(\text{C})$ (resulting from the spectrum fitting at 10680–10695.5 Å; where the best-fit over the whole region is accomplished by adjusting single carbon abundance), (2) atomic parameters ($\chi_{\text{low}} = 7.483$ eV and $\log gf = +0.076$ for this line; cf. table 2 in TTH13), and (3) the same ξ and the model atmosphere adopted in the spectrum-synthesis analysis.

This means that the correction of W'_λ is nothing but a simple multiplication by a constant factor of $1 + \alpha$, which equally applies to any spectrum of different μ (note that α is a spectrograph-specific quantity at a given wavelength range).

Now, regarding the apparent equivalent widths (W'_λ) of C I 10683, 10685, and 10691 lines measured by the method mentioned in subsection 2.2, we have (241.1, 178.7, and 304.8 mÅ) for the reference disk-center FTS spectrum and (196.7, 144.8, and 247.7 mÅ) for our DST spectrum at $\mu = 1$. Taking the former values as “true” equivalent widths according to assumption (ii), we obtain the W_λ/W'_λ ratios ($= 1 + \alpha$) for these three lines as 1.225, 1.234, and 1.231, which yield $\alpha = 0.23$ as an average.

This value was also checked from the viewpoint of spectrum matching. Following Allende Prieto et al. (2004) we simulated the line-weakening effect by adding constant scattered light (fraction α of the continuum intensity) to the reference FTS spectrum, which was further broadened corresponding to the difference of spectral resolution.⁶ We then found that $\alpha \sim 0.25$ (i.e., almost the same as 0.23 derived from W_λ) gives the best fit with our disk-center spectrum, as illustrated in figure 4.

Consequently, we adopted the following formula to obtain the corrected equivalent widths

$$W_\lambda(\mu) = 1.23 W'_\lambda(\mu) \quad (4)$$

for each of the C I lines. The finally resulting (corrected) $W_\lambda(\mu)$ values are summarized in table 1.⁷ Yet, we should keep in mind that derivation of these values is based on assumptions (i) and (ii), upon which their validity depends. Nevertheless, as discussed in appendix 1, we will see that our adopted W_λ values of O I 7771–5 triplet lines, for which the effect of scattered light has been corrected in a similar manner ($\alpha = 0.09$ in this case), are consistent with various published results (cf. figure 12). This fact may lend support for our treatment.

3. Computation of Line Strengths

3.1. Model Atmospheres and Microturbulence

In the calculation of theoretical equivalent widths (at various μ values on the solar disk) to be compared with the observational data in table 1, we closely followed the work of Takeda (1995b; hereinafter referred to as TAK95b) and tested two solar atmospheric models ($T_{\text{eff}} = 5780$ K, $\log g = 4.44$, $[\text{Fe}/\text{H}] = 0.0$) having different temperature profiles only at the upper layer of $\tau_{5000} \lesssim 10^{-4}$. Model C has a chromospheric temperature structure of Maltby et al.’s

⁶ Since the spectrum resolution of the FTS spectrum is $R_{\text{FTS}} \simeq 350,000$ and that of our DST spectrum is $R_{\text{DST}} \simeq 190,000$, we convolved $I(\lambda) + \alpha I_{\text{cont}}$ with a Gaussian function having a FWHM of $3 \times 10^5/R'$ km s⁻¹, where $R' (\simeq 230,000)$ was derived from the equation $1/R'^2 = 1/R_{\text{DST}}^2 - 1/R_{\text{FTS}}^2$.

⁷ For reference, Baschek and Holweger (1967) derived 189 mÅ and 281 mÅ for the disk-center equivalent widths of C I 10685 and 10691 lines, respectively. These are reasonably compared with our reference values of 178 mÅ and 305 mÅ.

(1986) semi-empirical photospheric reference model, while Model E is essentially equivalent to Kurucz’s (1979) ATLAS6 solar model (without any temperature rise). The pressure/density structures of these models were obtained by integrating the equation of hydrostatic equilibrium. See subsection 2.1 of TAK95b (and appendix 2 of this paper) for more details about how Models C and E were constructed.

Regarding the microturbulence (ξ), we examined two different models: (a) the depth-dependent microturbulent velocity field [$\xi_M(\tau)$; conspicuously increasing with height at $\tau_{5000} \lesssim 10^{-4}$] of the reference solar atmosphere empirically derived by Maltby et al. (1986; cf. their Table 11), and (b) a depth-dependent microturbulence of 1 km s^{-1} often adopted in spectroscopic studies of solar spectra (see, e.g., subsection 3.2 in Takeda 1994). The structures of $T(\tau)$, $P(\tau)$, and $n_e(\tau)$ for both Models C and E, along with two microturbulence models ($\xi_M(\tau)$ and $\xi = 1 \text{ km s}^{-1}$), are depicted in figure 5.

3.2. Non-LTE Calculations

The procedures of our non-LTE calculations are the same as adopted in TTH13. As mentioned in section 1, our main purpose is to examine whether the H I collision rates computed with the classical formula are reasonable or they need to be significantly revised. Therefore, as in TTH13, we write the total collisional rates (C_{total}) by introducing a correction factor (k_H) as

$$C_{\text{total}} = C_e + k_H C_H, \quad (5)$$

where C_e and C_H are the collisional rates due to electrons and neutral hydrogen atoms, respectively, computed in the standard recipe (cf. subsection 3.1 of TTH13).

Practically, we tried three k_H values (0.1, 1, and 10) in our calculations, in order to see how the results are influenced by changing this parameter. The way in which the line opacity (l_0) and the line source function (S_L) of the $3s \ ^3P^o - 3p \ ^3D$ transition (corresponding to C I 10683/10685/10691 lines) depend on the choice of k_H is displayed in figure 6. As recognized from this figure, the non-LTE effect is seen in the increase in the line opacity [$l_0(\text{NLTE})/l_0(\text{LTE}) > 1$] as well as in the dilution of the line source function ($S_L/B < 1$) in the line-forming regions; both act in the direction of intensifying the lines. This effect becomes progressively more conspicuous with a decrease in k_H , as naturally expected because a decrease in the collisional rates tends to enhance the departure from LTE.

4. Discussion

4.1. Effect of Atmospheric Structure

We first discuss the effects caused by different choices of solar atmospheric model as well as of microturbulence on the equivalent widths of C I lines computed at various μ values. Figure 7 shows the non-LTE W_λ vs. μ relations corresponding to $k_H = 1$, which were computed with a fixed carbon abundance for Model C (red thick lines) and Model E (blue thin lines) in

combination with $\xi = \xi_M(\tau)$ (solid lines) and $\xi = 1 \text{ km s}^{-1}$ (dashed lines). We can recognize the following characteristics from this figure:

— First, the difference between two microturbulence models, depth-dependent $\xi_M(\tau)$ and constant $\xi = 1 \text{ km s}^{-1}$, causes only insignificantly small changes in W_λ , which is presumably because that these two ξ models do not differ much from each other (in the average sense) at the important line-forming region ($10^{-3} \lesssim \tau_{5000} \lesssim 1$; cf. figure 5).

— Second, an appreciable difference is seen between the results of Model C and Model E; that is, $W_\lambda(\text{C})$ tends to be larger than $W_\lambda(\text{E})$, and the difference systematically increases toward the limb (i.e., with a decrease in μ). This is just the same tendency found in the case of O I 7771–5 triplet lines as pointed out by TAK95b (cf. figure 12 therein). Since C I 10683/10685/10691 lines and O I 7771–5 lines share the similar characters to each other (i.e., strong high-excitation lines of multiplet 1 originating from a metastable term), this trend can be interpreted as due to the same mechanism working for those O I lines (i.e., shift of the core forming region upward into the higher layer where the line source function is more diluted, since the line opacity is enhanced due to the temperature rise; cf. subsection 2.4 in TAK95b).

4.2. Influence of Changing k_H

The effect of changing k_H is demonstrated in figure 8, where the W_λ vs. μ relations for the representative C I 10683 line, corresponding to $k_H = 0.1, 1, 10, \text{ and } \infty$ (LTE), are depicted for two solar model atmospheres; Model C with $\xi = \xi_M(\tau)$ and Model E with $\xi = 1 \text{ km s}^{-1}$. It can be seen from figure 8a (fixed carbon abundance) that W_λ at a given μ tends to increase with a decrease in k_H , since the non-LTE effect (being enhanced with a lowered k_H) always acts in the direction of strengthening a line as explained in subsection 3.2. This effect becomes more appreciable for smaller μ (toward the limb), because the line-forming region systematically moves toward an upper layer with a decrease in μ where the non-LTE effect is stronger. This figure also exhibits the effect of $T(\tau_{5000})$ structure mentioned in the previous subsection; i.e., the inequality relation of $W_\lambda(\text{C}) > W_\lambda(\text{E})$ at a given μ and k_H .⁸

In comparing the results calculated with various conditions with observations, it is necessary to appropriately adjust the carbon abundance at the disk center so that the condition $W_\lambda^{\text{cal}}(\mu = 1) = W_\lambda^{\text{obs}}(\mu = 1)$ holds for each case. Such normalized W_λ vs. μ relations after this matching has been applied are presented in figure 8b, where we can see that the gradient $|dW_\lambda/d\mu|$ is lessened with a lowering of k_H , reflecting the that non-LTE intensification of W_λ is enhanced with decreasing μ toward the limb. This characteristics may be used to give a constraint on k_H in comparison with the observed μ -dependence of W_λ .

⁸ Note that this inequality exceptionally breaks down for the case of LTE, where $W_\lambda(\text{C}) < W_\lambda(\text{E})$ holds especially near to the limb, since the chromospheric temperature rise in Model C causes a core emission in the line profile when computed with LTE, which eventually makes the equivalent width smaller.

4.3. Comparison with Observations and Conclusion

We are now ready to get empirical information on k_{H} by comparing the theoretical and observed W_{λ} vs. μ relations: the primary aim of this study. Here, we exclusively adopt Model C with $\xi = \xi_{\text{M}}(\tau)$ as the standard solar atmospheric model since it is considered to be comparatively more realistic, while keeping in mind that an application of Model E causes a marginal increase in the gradient $|dW_{\lambda}/d\mu|$ (i.e., equivalent to an increase in k_{H}) as compared to the case of Model C (cf. figure 8b).

Our results are shown in figure 9, where the observed center-to-limb variations of W_{λ} for C I 10683/10685/10691 lines are overplotted with the theoretical relations corresponding to $k_{\text{H}} = 0.1, 1, 10,$ and ∞ (LTE). This figure indicates that the observed data are almost consistent with the relations for $k_{\text{H}} = 1$ in the average/global sense (especially based on the matching at $0.6 \gtrsim \mu \gtrsim 0.3$), though it is difficult to establish an exact solution because of the rather large scatter comparable to the difference caused by changing k_{H} . We may thus state that non-LTE calculations using the H I collision rates evaluated with the formula based on the classical cross section can reasonably reproduce the observed W_{λ} vs. μ relations of these C I lines, which means that the necessity of significantly revising these classical C_{H} rates (e.g., considerable reduction, as occasionally argued) is unlikely. This is the conclusion of this investigation.

4.4. Implication and Problems

This consequence has a significant implication on carbon abundance determinations in very metal-poor stars. TTH13 found that C abundances derived from CH lines tend to be smaller than those derived from C I 10683/10685/10691 lines by several tenths dex for stars at $[\text{Fe}/\text{H}] \lesssim -2$. One possible scenario that might explain this discrepancy was to considerably reduce k_{H} (from the value of unity assumed in TTH13), since it would further lower the C I abundance (due to an enhanced non-LTE effect) in the direction of mitigating the discordance. Now that this possibility has been ruled out, we feel that this disagreement between C I and CH abundances may be rather attributed to an underestimation of the latter, since molecular lines are considerably sensitive to temperature structures of upper layers and apt to be unreliable.

Here, a remark of caution may be relevant. It may still be rather premature to regard this consequence as conclusive. We should realize that our result is based on a classical Kurucz's (1979) solar atmospheric model (though the chromospheric effect was taken into account by referring to Maltby et al.'s model), while other published photospheric models have slightly different structures from that we adopted (cf. appendix 2). In appendix 1, the k_{H} value relevant for O I 7771–5 lines is discussed from the μ -dependence of W_{λ} , where our theoretical calculations are done with the same solar model atmosphere. As we will see, we obtained a result discrepant from that obtained recently by Pereira et al. (2009b) based on their state-of-art 3D dynamical solar model atmosphere. It is interesting to see, therefore, how the present result may be influenced by applying this kind of new approach. Yet, since the use of such

a realistic 3D model tends to raise the theoretical W_λ of these C I lines (i.e., equivalent to decreasing k_H) according to Asplund et al. (2005), which is also expected from the case of O I 7771–5 lines having similar excitation potentials (cf. figure 5 in Pereira et al. 2009b), its application would act in the direction of increasing the empirical solution for k_H . This makes the possibility of reducing k_H even more unlikely.

Finally, we should recall that our adopted equivalent widths were derived by applying appreciable scattered light corrections. Thus, follow-up independent observations of center-to-limb variations of these C I 1.07 μm lines (preferably with an instrument such as FTS) would be desired to check our correction procedure.

Appendix 1. Center-to-Limb Variation of O I 7771–5 Å Lines

On the same day of 2013 July 26 when our solar spectroscopic observations of C I 10683/10685/10691 lines were carried out, we also observed the O I 7771–5 triplet lines, which share similar characters to those of C I lines (e.g, strong lines of multiplet 1 originating from high-excited metastable term). This is because we want to check our observation and data reduction process (especially in terms of the procedure for scattered-light correction), since empirical W_λ vs. μ relations for these O I lines have already been published by several investigators and can be compared with ours.

We found that the lines in our disk-center spectrum are generally weaker than the reference FTS spectrum also for this case of O I lines as shown in figure 10, though the extent of weakening is comparatively milder than the case of C I lines, which indicates that the effect of scattered light in our instrument becomes more appreciable with increasing wavelength. Since the apparent equivalent widths (W'_λ) of these O I 7771, 7774, and 7775 lines evaluated in the same way using synthetic spectrum fitting (cf. figure 11) as described in subsection 2.2 turned out to be (83.6, 72.1, and 57.1 mÅ) for the reference disk-center FTS spectrum and (77.1, 66.2, and 52.0 mÅ) for our DST spectrum at $\mu = 1$, the resulting W_λ/W'_λ ratios ($= 1 + \alpha$) are 1.084, 1.089, and 1.098, respectively, which yield $\alpha = 0.09$ as an average. Accordingly, we multiplied the apparent W'_λ values by a correction factor of 1.09 to obtain the final equivalent widths, which are summarized in table 2.

These W_λ results are plotted against μ in figure 12, where the published values taken from various literature are also shown. We can state by inspecting this figure that the equivalent widths derived from our observation are mostly in reasonable agreement with those published ones, which may justify our measurement as well as the correction procedure for stray light.

In analogy with figure 9, theoretical relations for these O I 7771–5 lines corresponding to $k_H = 0.1, 1, 10,$ and ∞ (LTE) computed for Model C with $\xi = \xi_M(\tau)$ are also depicted in figure 12. This figure indicates that all these theoretical W_λ vs. μ relations calculated for three k_H values situate below the observed data; i.e., we would have to require $k_H < 0.1$ in order to bring theory and observation into agreement. This is incompatible with the consequence

of TAK95a, where $k_{\text{H}} \sim 1$ was suggested based on the requirement of abundance consistency between O I 7771–5 lines and other O I lines (see also Takeda & Honda 2005; cf. appendix 1 therein). Actually, TAK95a could not reproduce the observed W_{λ} vs. μ relation for the O I 7771 line quantitatively well by his non-LTE calculations done with $k_{\text{H}} = 1$, though he pointed out that inclusion of chromospheric temperature rise can somewhat mitigate the discrepancy (cf. figure 12 therein). Thus, we must admit that there is still a disagreement in the value of k_{H} for the O I 7771–5 lines between these two approaches, as far as our adopted model atmosphere is concerned.⁹

Nevertheless, this problem may be resolved by applying different models, since the result seems sensitive to adopted atmospheric structures. For example, Pereira et al. (2009b) showed that the choice of $k_{\text{H}} \simeq 1$ can accomplish the best agreement between theoretical and observed center-to-limb variations of O I 7771–5 lines when their sophisticated 3D hydrodynamical model was used,¹⁰ while no solution could be obtained ($k_{\text{H}} < 0.01$, just like our case) when Gustafsson et al.’s (2008) 1D MARCS model was used. Figure 5 of Pereira et al. (2009b) illustrates this situation, where we can confirm that our figure 12b is quite similar to the upper-left panel (corresponding to MARCS model) of their figure 5. Therefore, the circumstance is rather complicated depending on the adopted model atmosphere, which led us to remark in subsection 4.4 that applying the new 3D model atmosphere would be desirable to check our conclusion.

Appendix 2. Comparison of Temperature Structures of Various Solar Photospheric Models

As in TAK95b, the solar model atmospheres adopted in this study (Model E and Model C) are based on Kurucz’s (1979) theoretical model computed by his ATLAS6 program, where the convection was taken into account by the local mixing-length theory with $l = 2H_{\text{p}}$ (H_{p} : pressure scale height). That is, this ATLAS6 solar model atmosphere (defined at $-4 \lesssim \log \tau_{5000}$) was simply extrapolated at $-7 \lesssim \log \tau_{5000} \lesssim -4$ for Model E, while the chromospheric $T(\tau_{5000})$ structure of Maltby et al.’s (1986) photospheric reference model was assumed at $-7 \lesssim \log \tau_{5000} \lesssim -4$ (and the hydrostatic equation was integrated to obtain the pressure structure) for Model C.

As shown in this study as well as in TAK95b, the difference in the structure of upper

⁹ However, based on Kurucz’s (1993) “non-overshooting” ATLAS9 model (which should not be so different from our adopted model), Allende Prieto et al. (2004) reported that $k_{\text{H}} = 1$ (rather than $k_{\text{H}} = 0$) better reproduces the observed W_{λ} vs. μ relation of the O I 7771–5 lines (cf. their figure 6), which contradicts our result. Though the reason is not clear, some difference might exist between our and their non-LTE calculation procedures.

¹⁰ Interestingly, the application of Holweger and Müller’s (1974) empirical solar model seems to yield a result similar to the case of the recent 3D model, as seen from the comparison of Pereira et al.’s (2009b) figures 4 (upper-middle panel) and 5 (upper-right panel).

optically-thin layer (i.e., between Model E and Model C) does not necessarily have so large impact on the resulting W vs. μ relations of C I 10683/10685/10691 and O I 7771/7774/7775 lines in the quantitative sense, though the changes are surely appreciable.

On the other hand, the temperature structure of deeper photospheric layers is considered to influence more significantly on the formation of these C I and O I lines of high-excitation. Actually, as seen from the distribution of contribution function of these lines, most contribution comes from $-1 \lesssim \log \tau_{5000} \lesssim +0.5$ (cf. figure 7 of Takeda 1994 for the case of disk center, though the formation layer is systematically shifted upward at the limb). Accordingly, it is worthwhile to examine how the photospheric $T(\tau_{5000})$ structure of Kurucz's (1979) ATLAS6 model, on which our Model E and Model C are based, are compared with those of other representative solar model atmospheres published so far.

Such comparisons of temperature structures of different solar photospheric models are displayed in figure 13, where Holweger and Müller's (1974) empirical model, Kurucz's (1979) theoretical ATLAS6 model, Maltby et al's (1986) semi-empirical photospheric reference model, Gustafsson et al.'s (2008) theoretical MARCS model, Kurucz's (1993) theoretical ATLAS9 model (with convective overshooting), and the new 3D dynamical model used by Pereira et al. (2009b) (averaged $\langle T(\tau_{5000}) \rangle$) are compared with each other.

An inspection of this figure suggests that the $T(\tau_{5000})$ structures of these models do not differ so much (differences are on the order of ~ 100 K) except for the convection-dominated deeper layer ($\log \tau_{5000} \gtrsim +0.5$). Yet, it should be realized that a temperature change of ~ 100 K suffices to cause an appreciable effect on the strength of these high-excitation C I and O I lines in question, as can be recognized from Pereira et al's (2009b) results for oxygen lines. In this sense, which solar photospheric model to choose is an important factor to be kept in mind when interpreting or discussing the matching of theoretical/empirical W vs. μ relation.

References

- Allende Prieto, C., Asplund, M., & Fabiani Bendicho, P. 2004, *A&A*, 423, 1109
 Altrrock, R. C. 1968, *Solar Phys.*, 5, 260
 Asplund, M., Grevesse, N., Sauval, A. J., Allende Prieto, C., & Blomme, R. 2005, *A&A*, 431, 693
 Baschek, B., & Holweger, H. 1967, *Z. Astrophys.*, 67, 143
 Drawin, H. W. 1968, *Z. Phys.*, 211, 404
 Drawin, H. W. 1969, *Z. Phys.*, 225, 483
 Gustafsson, B., Edvardsson, B., Eriksson, K., Jørgensen, U. G., Nordlund, Å., & Plez, B. 2008, *A&A*, 486, 951
 Holweger, H., & Müller, E. A. 1974, *Solar Phys.*, 39, 19
 Kurucz, R. L. 1979, *ApJS*, 40, 1
 Kurucz, R. L. 1993, Kurucz CD-ROM No.13 (Smithsonian Astrophysical Observatory)
 Maltby, P., Avrett, E. H., Carlsson, M., Kjeldseth-Moe, O., Kurucz, R. L., & Loeser, R. 1986, *ApJ*,

306, 284

Müller, E. A., Baschek, B., & Holweger, H. 1968, *Solar Phys.*, 3, 125

Nakai, Y., & Hattori, A. 1985, *Mem. Fac. Sci., Kyoto Univ., Ser. A, Phys., Astrophys., Geophys. Chem.*, 36, 385

Neckel, H. 1994, in *The Sun as a Variable Star, Solar and Stellar Irradiance Variations*, IAU Coll. 143, ed. J. M. Pap, C. Frolich, H. S. Hudson, & S. Solanki (Cambridge: Cambridge University Press), p. 37

Neckel, H. 1999, *Solar Phys.* 184, 421

Pereira, T. M. D., Asplund, M., & Kiselman, D. 2009b, *A&A*, 508, 1403

Pereira, T. M. D., Kiselman, D., & Asplund, M. 2009a, *A&A*, 507, 417

Steenbock, W., & Holweger, H. 1984, *A&A*, 130, 319

Takeda, Y. 1994, *PASJ*, 46, 53

Takeda, Y. 1995a, *PASJ*, 47, 287

Takeda, Y. 1995b, *PASJ*, 47, 463 (TAK95b)

Takeda, Y., & Honda, S. 2005, *PASJ*, 57, 65

Takeda, Y., & Takada-Hidai, M. 2013, *PASJ*, 65, 65 (TTH13)

Table 1. Equivalent widths of C I 10683.08, 10685.34, and 10691.24 lines at various μ points on the solar disk.

d (R_0)	μ	W_{10683} (mÅ)	W_{10685} (mÅ)	W_{10691} (mÅ)
0.00	1.000	242	178	305
0.45	0.893	220	161	277
0.50	0.866	224	164	282
0.55	0.835	222	163	280
0.60	0.800	219	160	275
0.65	0.760	214	157	270
0.70	0.714	210	154	265
0.75	0.661	213	156	269
0.80	0.600	198	144	250
0.85	0.527	191	139	241
0.90	0.436	194	141	245
0.95	0.312	174	125	220

Note.

Given here are the finally adopted values after being corrected for the effect of scattered light by multiplying the correction factor of 1.23. (The directly measured raw equivalent widths are obtained by dividing these values by the same factor.) The apparent distance d on the solar disk between the observed point and the disk center (in unit of R_0 , the apparent radius of the disk) is connected with μ ($\equiv \cos \theta$; direction cosine) by the relation $\mu = \sqrt{1 - d^2}$.

Table 2. Equivalent widths of O I 7771.94, 7774.17, and 7775.39 lines at various μ points on the solar disk.

d (R_0)	μ	W_{7771} (mÅ)	W_{7774} (mÅ)	W_{7775} (mÅ)
0.00	1.000	84	72	57
0.45	0.893	81	70	55
0.50	0.866	79	68	53
0.55	0.835	78	67	53
0.60	0.800	77	66	52
0.65	0.760	77	66	52
0.70	0.714	75	64	50
0.75	0.661	72	62	48
0.80	0.600	72	62	48
0.85	0.527	67	57	44
0.90	0.436	63	54	42
0.95	0.312	61	51	40

Note.

Given here are the finally adopted values after being corrected for the effect of scattered light by multiplying the correction factor of 1.09. (The directly measured raw equivalent widths are obtained by dividing these values by the same factor.)

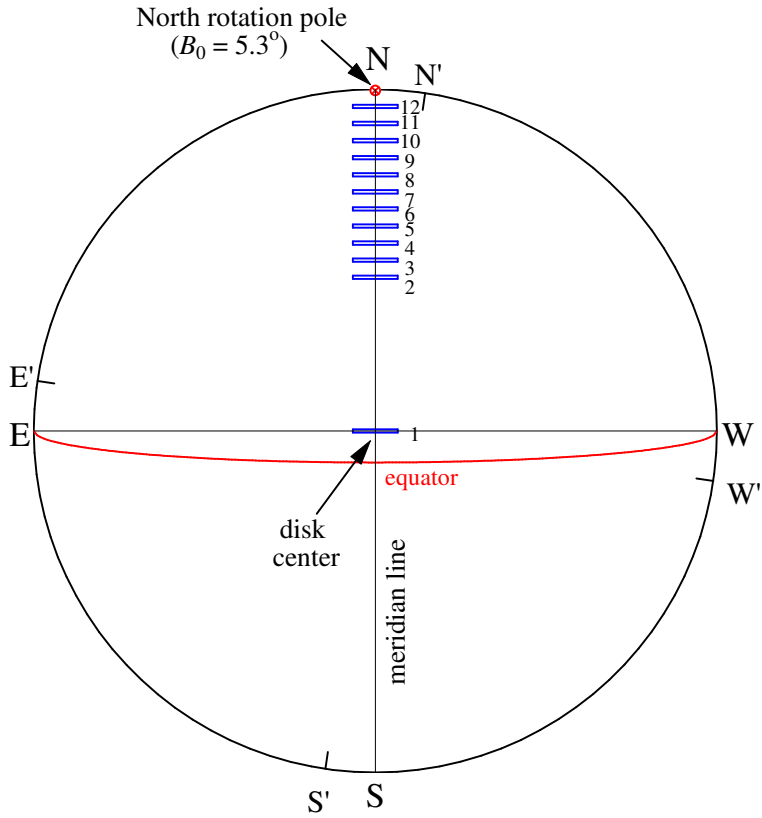


Fig. 1. Observed 12 points on the meridian line of the solar disk (1 point at the disk center and 11 points from $0.45 R_0$ to $0.95 R_0$ with a step of $0.05 R_0$, where R_0 is the apparent radius of the solar disk), at which the slit was aligned in the E-W direction. While N, S, E, and W are the directions in reference to the Sun (based on solar rotation), those in the equatorial coordinate system on the celestial sphere (defined by the rotation of Earth) are also denoted as N' , S' , E' , and W' .

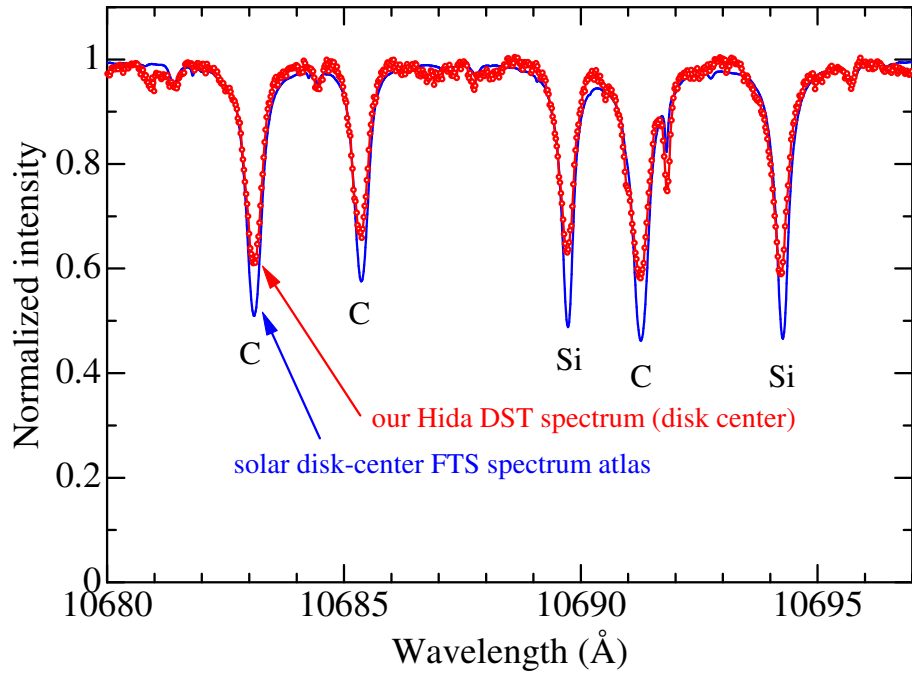


Fig. 2. Comparison of our 10680–10697 Å region spectrum (comprising C I and Si I lines) at the disk center with that of solar disk-center FTS spectrum atlas (Neckel 1994, 1999), where the former is displayed in (red) open circles connected by lines and the latter is in (blue) solid lines.

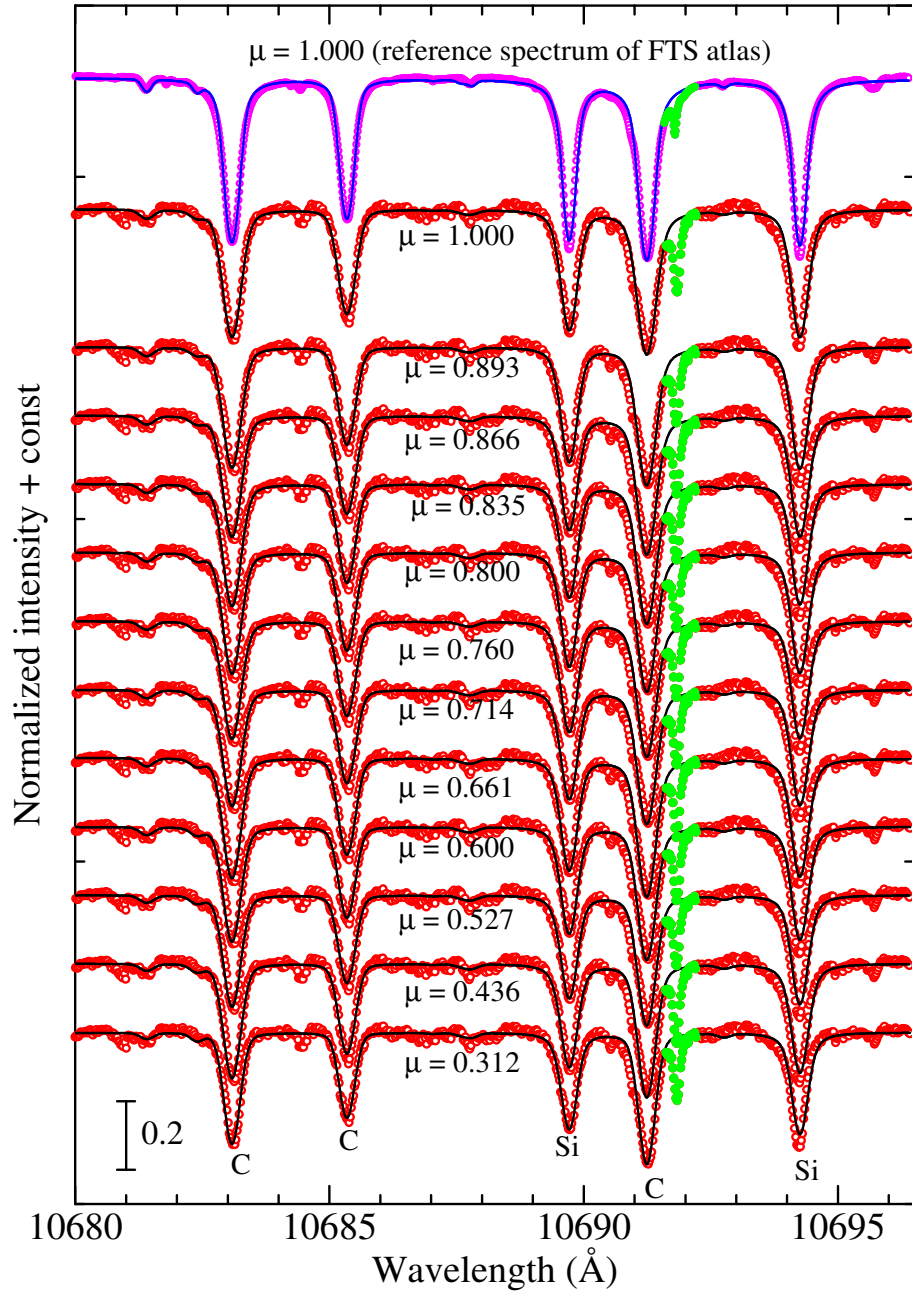


Fig. 3. Synthetic spectral fitting for each spectrum of different μ accomplished by finding the best-match abundance solution of C (and Si), from which the equivalent widths of C I 10683/10685/10691 lines were inversely computed. The theoretical spectra are shown by solid lines while the observed data are plotted by circles (where those of telluric origin and masked in the fitting are highlighted in green). Following the reference FTS spectrum displayed at the top, our DST spectra are arranged in the descending order of μ with appropriate offsets relative to the adjacent ones.

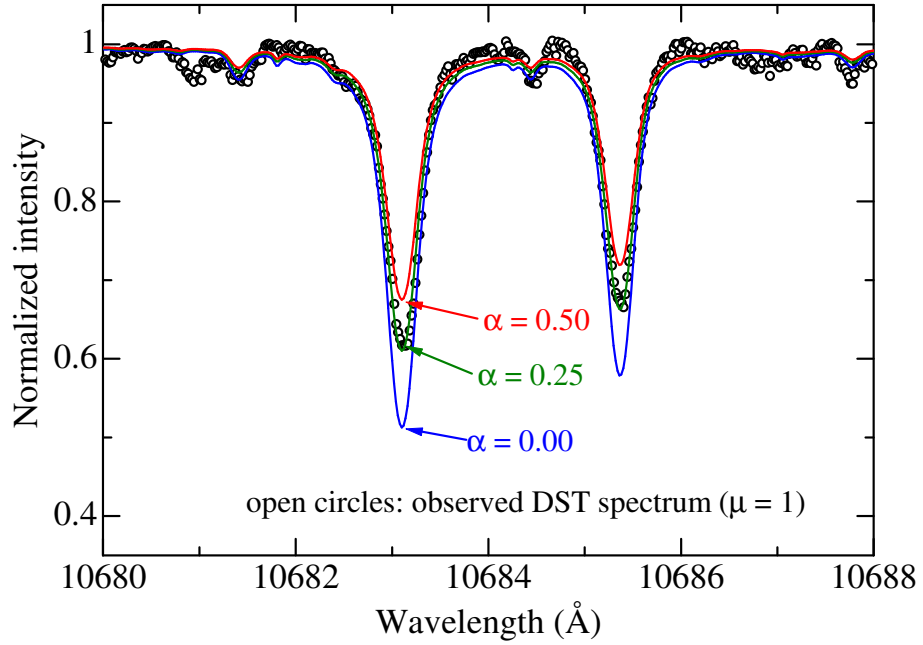


Fig. 4. Simulation of how the inclusion of scattered light affects the profiles of C I 10683 and 10685 lines in the disk-center spectrum. The three solid lines show the simulated spectra computed based on the reference solar disk-center FTS spectrum, to which three values of scattered light (fraction α of the continuum intensity; $\alpha = 0.00, 0.25,$ and 0.50 are colored in blue, green, and red, respectively) were added and an appropriate broadening was applied to take into account the difference of spectral resolution (see subsection 2.3). Our DST spectrum ($\mu = 1$) is also shown for comparison (open circles).

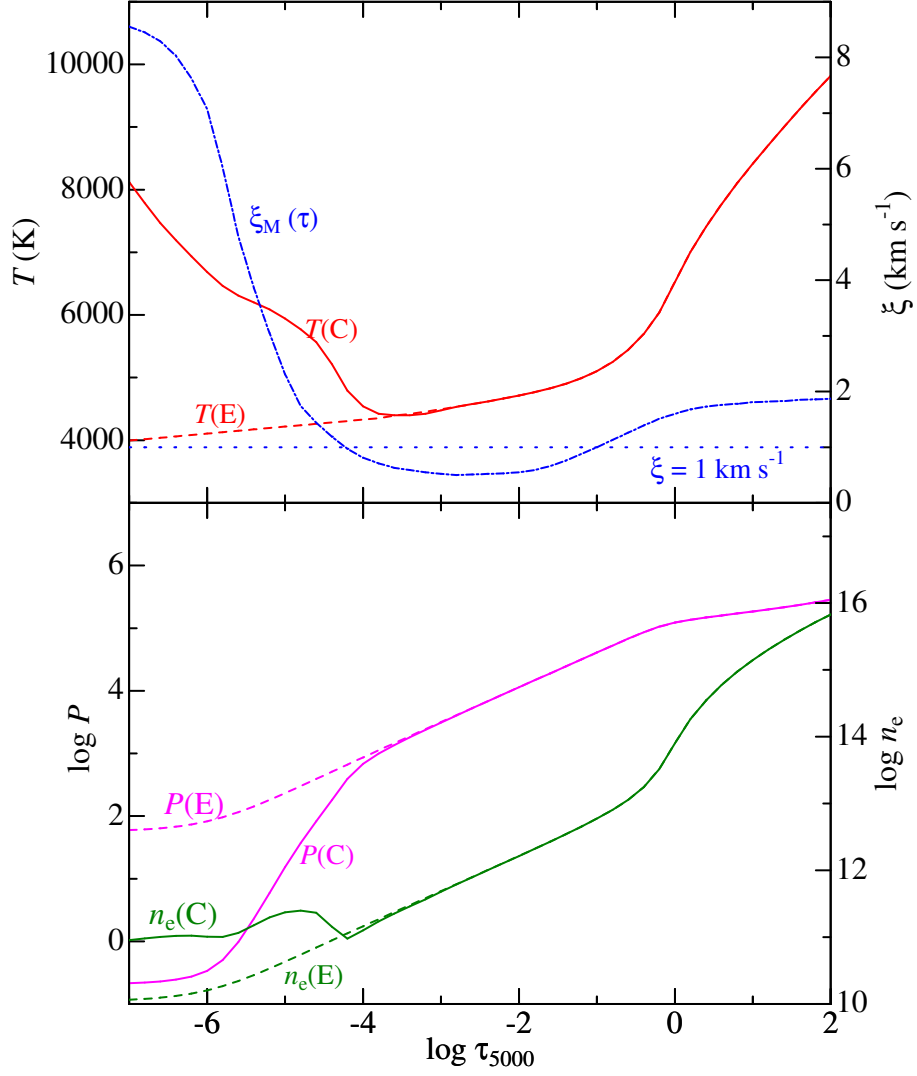


Fig. 5. Distributions of T (temperature), P (pressure), and n_e (electron density) plotted against $\log \tau_{5000}$ for two solar atmospheric models, Model C (solid lines) and Model E (dashed lines), used in this study (cf. subsection 3.1). In addition, Maltby et al.'s (1986) depth-dependent microturbulence [$\xi_M(\tau)$; dash-dotted line] for the reference solar atmosphere is compared with the occasionally used (depth-independent) value of $\xi = 1 \text{ km s}^{-1}$ (dotted line).

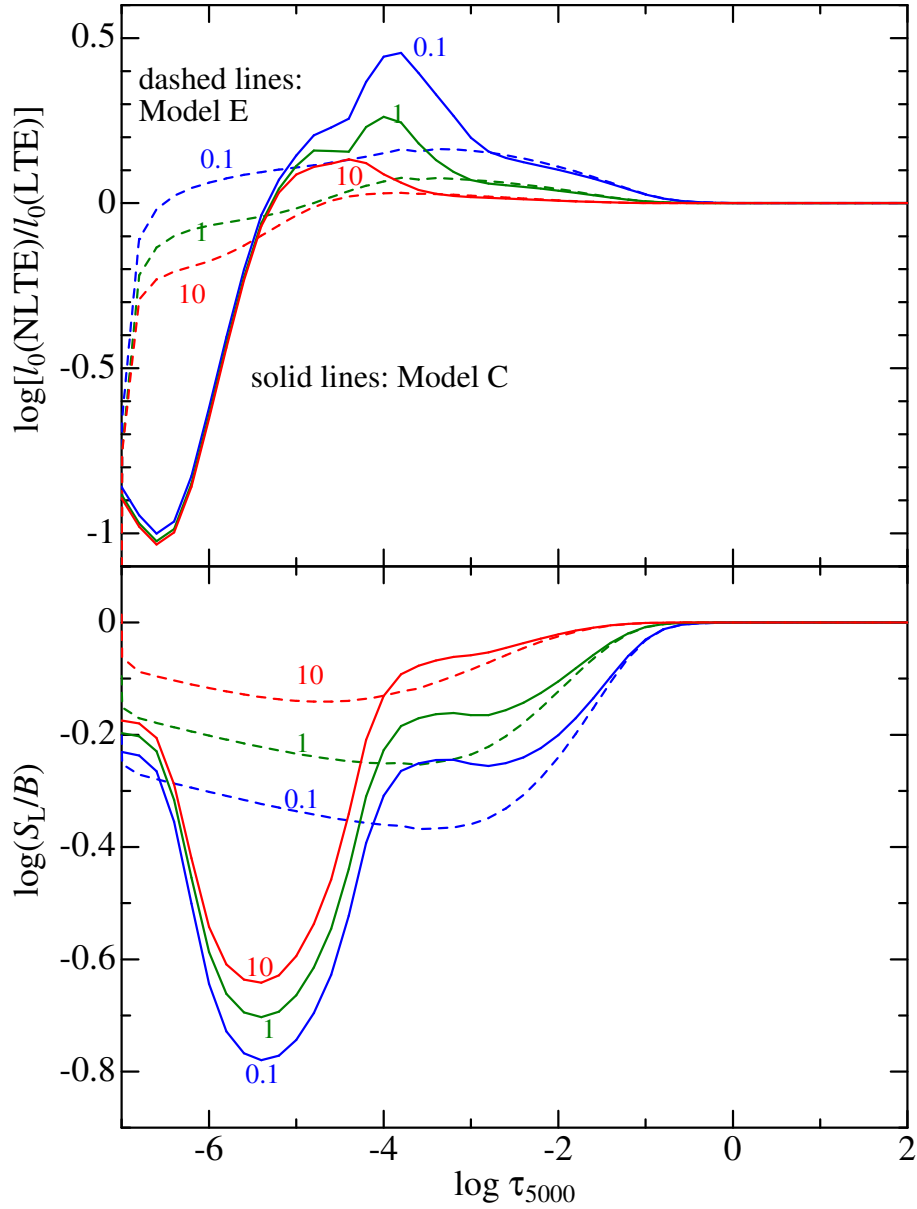


Fig. 6. Depth-dependence of the non-LTE to LTE opacity ratio (upper panel) as well as of the line source function (S_L) in unit of the local Planck function (B) (lower panel), calculated for three κ_H values (0.1, 1, and 10) as indicated in the figure. The results for Model C are depicted in solid lines, while those for Model E are in dashed lines.

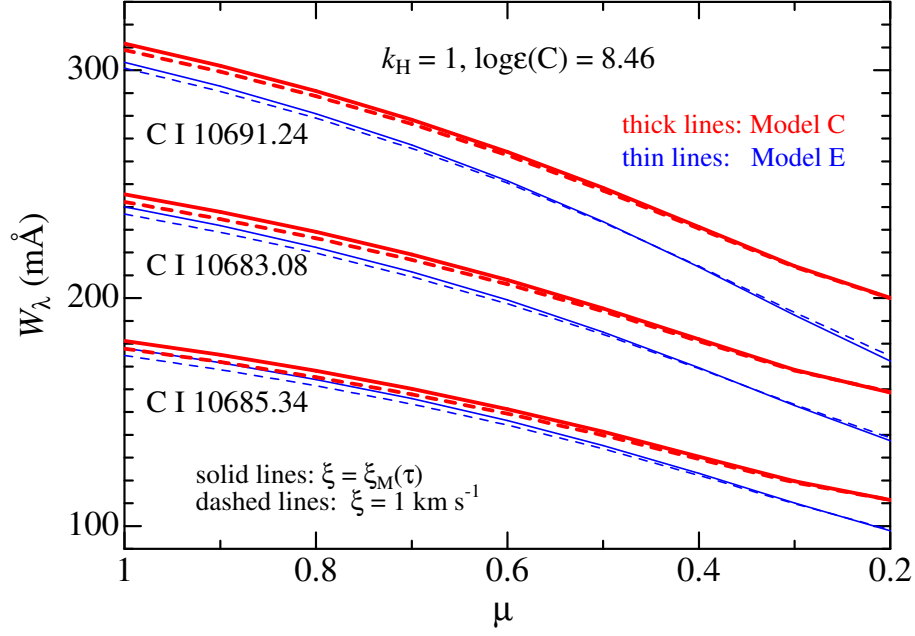


Fig. 7. Demonstration of how the difference in the model structure or in the microturbulence affects on the W_λ vs. μ relations of C I 10683/10685/10691 lines. Presented are the non-LTE results corresponding to $k_H = 1$, which were computed with $\log \epsilon(C) = 8.46$ for Model C (red thick lines) and Model E (blue thin lines) in combination with $\xi = \xi_M(\tau)$ (solid lines) and $\xi = 1 \text{ km s}^{-1}$ (dashed lines).

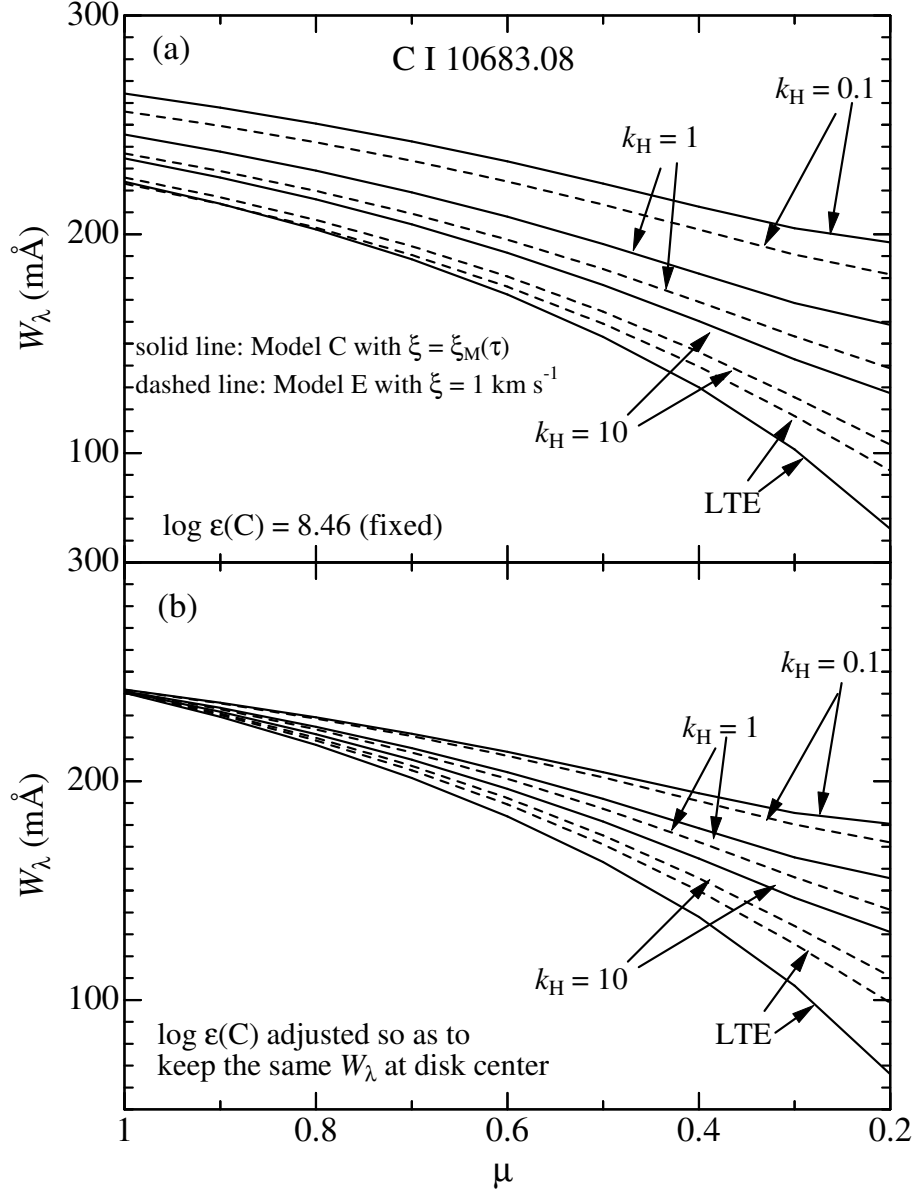


Fig. 8. Demonstration of how the change in k_H affects on the W_λ vs. μ relation of the representative C I 10683.08 line. Computations were done for $k_H = 0.1, 1, 10$, and ∞ (LTE) as indicated in the figure. The results for Model C with $\xi = \xi_M(\tau)$ are shown in solid lines, and those for Model E with $\xi = 1 \text{ km s}^{-1}$ are in dashed lines. The relations derived for a fixed carbon abundance of $\log \epsilon(\text{C}) = 8.46$ are presented in the upper panel (a), while those obtained with appropriately adjusted carbon abundances (to keep $W_\lambda(\mu = 1)$ at the same value of 242 mÅ) are given in the lower panel (b).

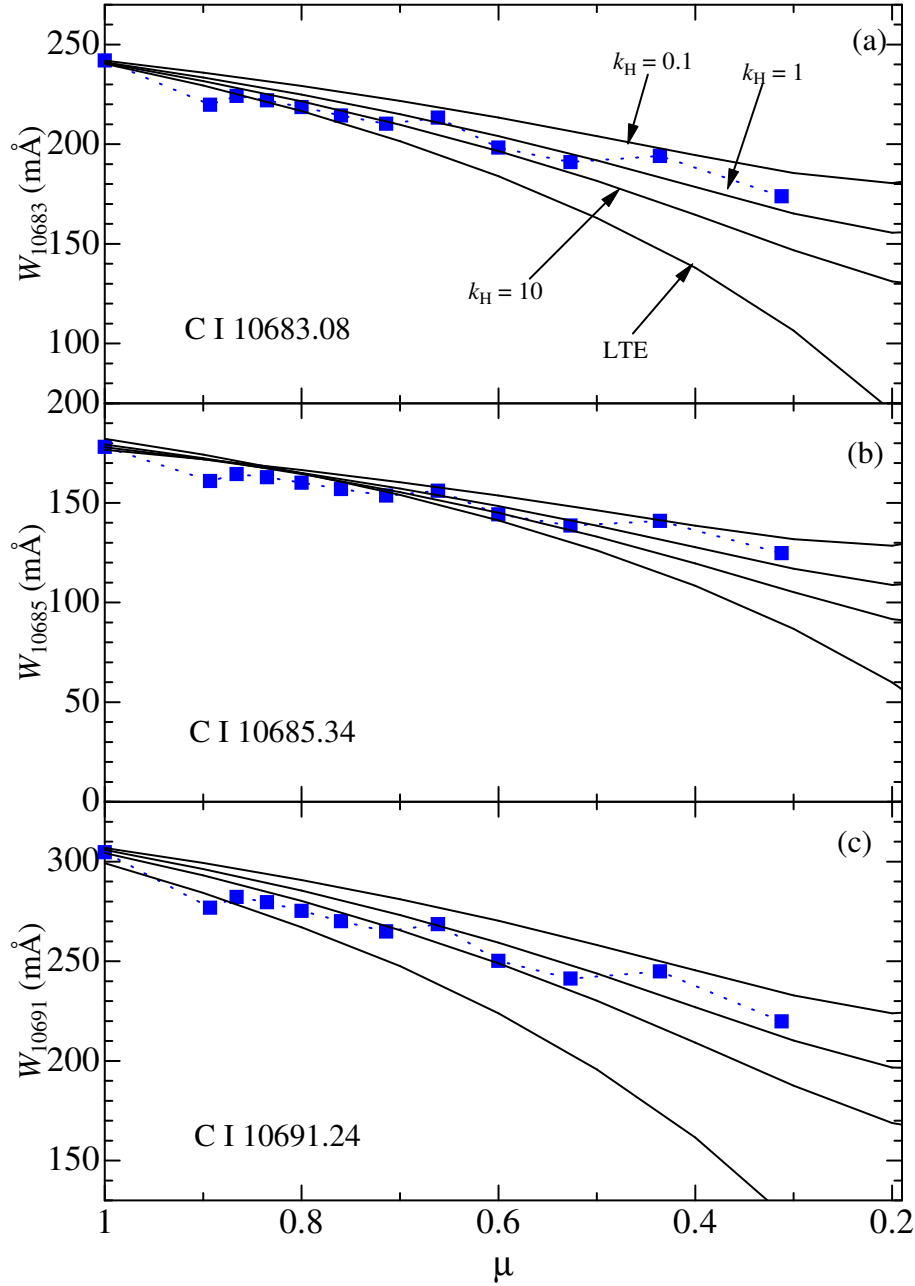


Fig. 9. Comparison of the theoretical W_λ vs. μ relations (solid lines) computed for Model C with $\xi = \xi_M(\tau)$ with the observed center-to-limb variation of the equivalent widths (filled squares; cf. table 1). Panels (a), (b), (c) present the results for C I 10683.08, 10685.34, and 10691.24 lines, respectively. Calculations were done for $k_H = 0.1, 1, 10$, and ∞ (LTE) (generally, W_λ decreases with an increase in k_H at a given μ) as indicated in the figure, and the abundances were adequately adjusted each case so as to make the computed $W_\lambda(\mu = 1)$ almost consistent with the observed disk-center values.

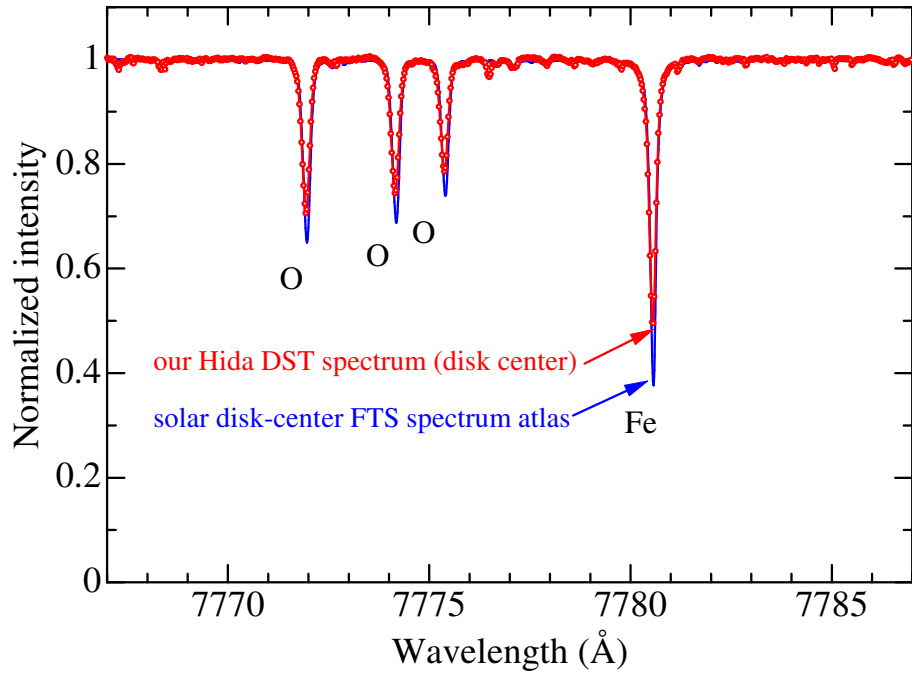


Fig. 10. Comparison of our 7767–7787 Å region spectrum (comprising O I and Fe I lines) at the disk center with that of solar disk-center FTS spectrum atlas. Otherwise, the same as in figure 2.

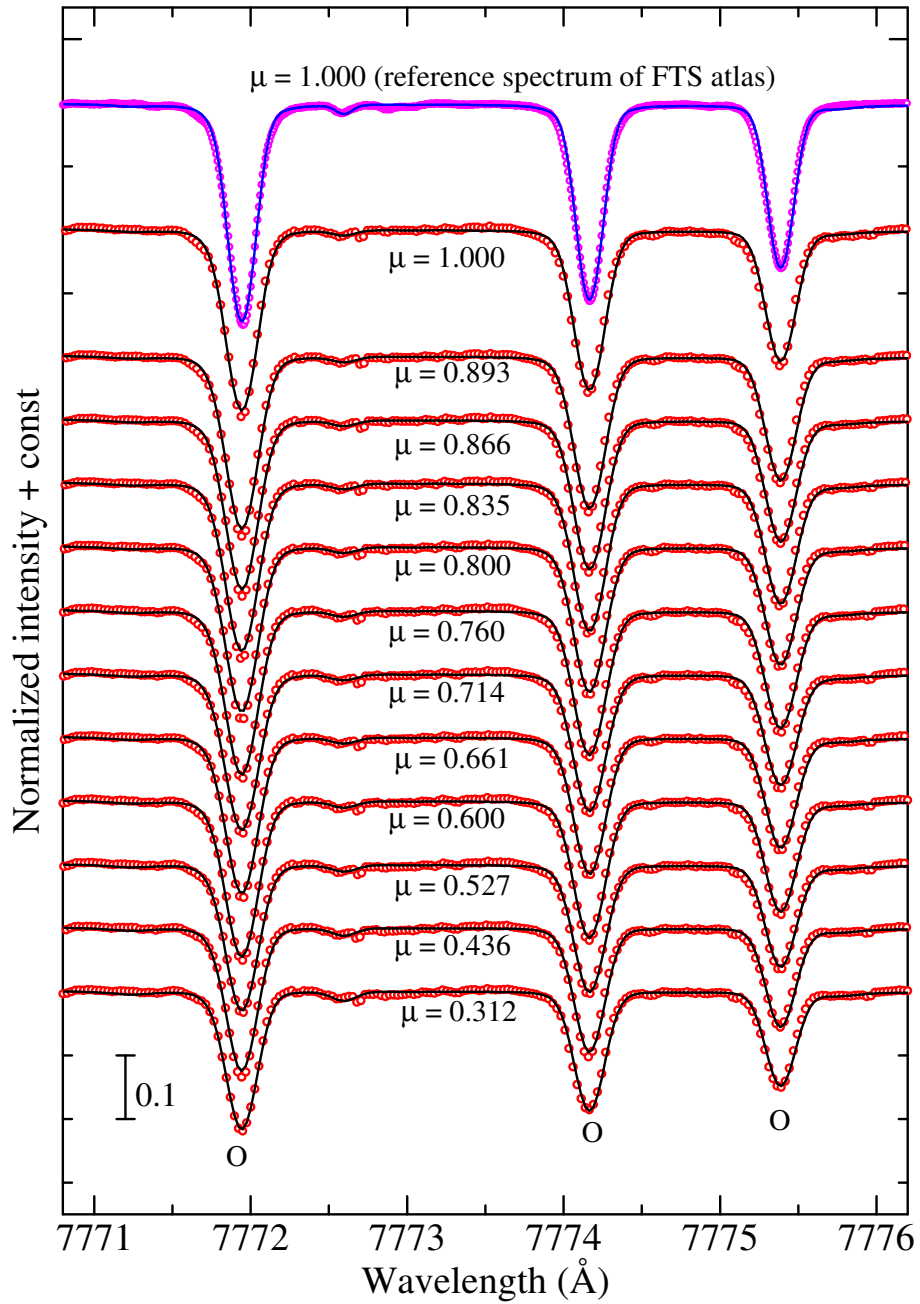


Fig. 11. Synthetic spectral fitting for each spectrum of different μ accomplished by finding the best-match abundance solution of O, from which the equivalent widths of O I 7771/7774/7775 lines were inversely computed. Otherwise, the same as in figure 3.

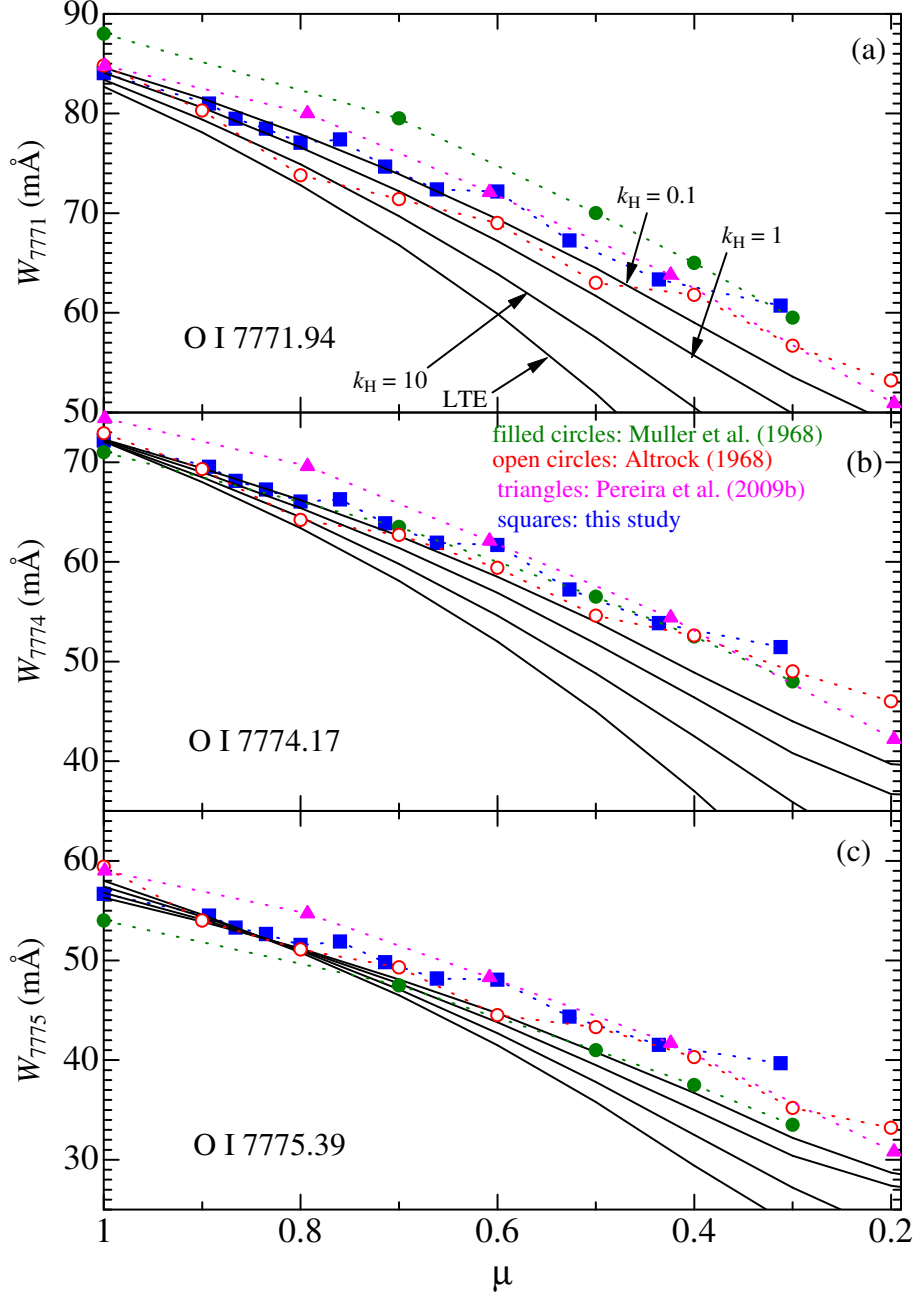


Fig. 12. Comparison of the theoretical W_λ vs. μ relations (solid lines) computed for Model C with $\xi = \xi_M(\tau)$ with the observed center-to-limb variation of the equivalent widths collected from various literature: Filled circles ... Müller et al. (1968), open circles ... Altrock (1968), filled triangles ... Pereira et al. (2009b), and filled squares ... our measurements. Panels (a), (b), (c) present the results for O I 7771.94, 7774.17, and 7775.39 lines, respectively. Otherwise, the same as in figure 9.

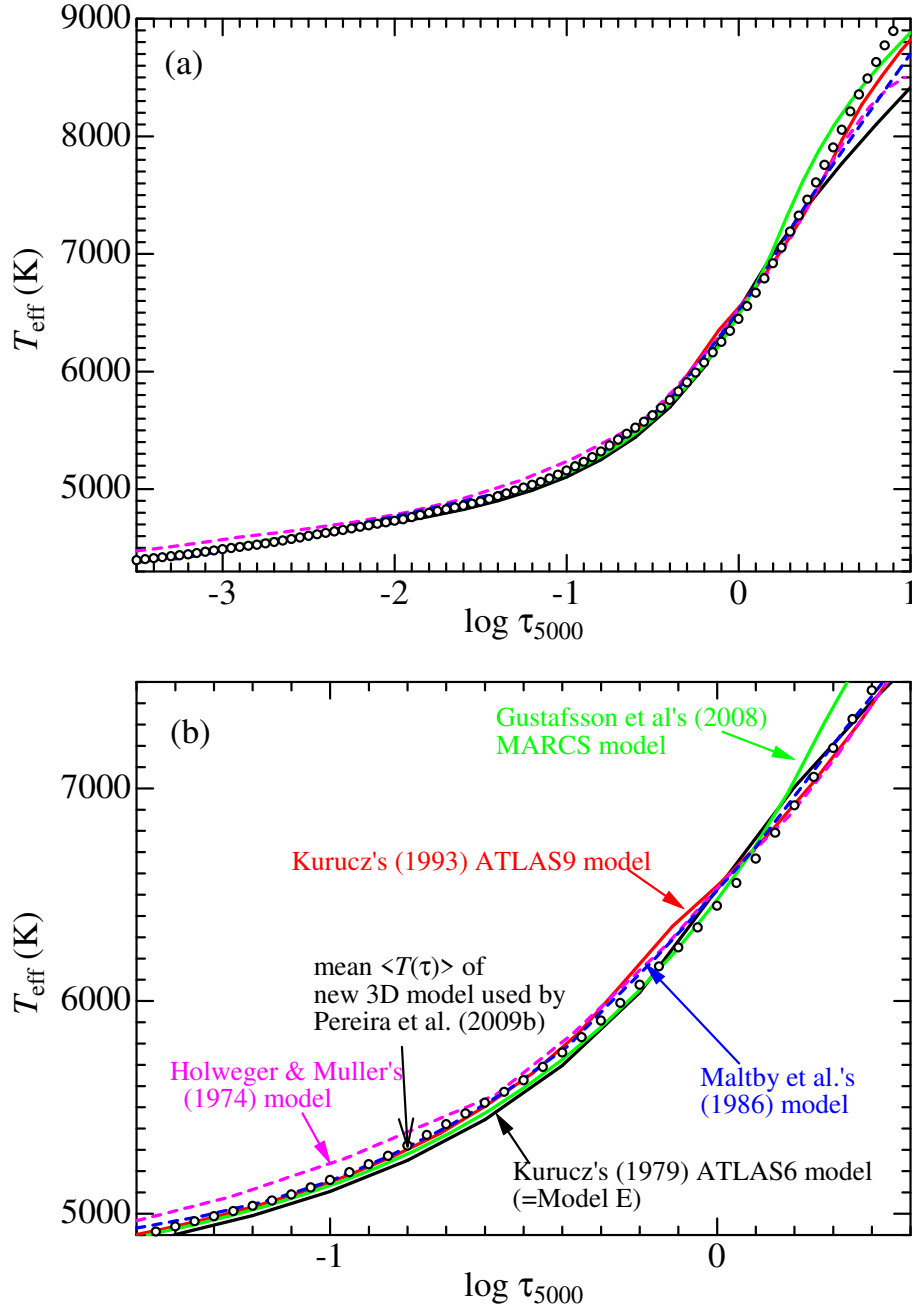


Fig. 13. Comparison of the temperature structures of different solar photospheric models. The upper panel (a) shows the T vs. τ_{5000} relation for the $-3.5 \leq \log \tau_{5000} \leq +1.0$ region (wide view), while the lower panel is for the $-1.5 \leq \log \tau_{5000} \leq +0.5$ region (zoomed view). Pink dashed line \cdots Holweger and Müller's (1974) model, black solid line \cdots Kurucz's (1979) ATLAS6 model (on which our Models E and C are based), blue dashed line \cdots Maltby et al.'s (1986) model, red solid line \cdots Kurucz's (1993) ATLAS9 model (with convective overshooting), light-green solid line \cdots Gustafsson et al.'s (2008) MARCS model, and open circles \cdots mean $\langle T(\tau_{5000}) \rangle$ of the new 3D model used by Pereira et al. (2009b) (read from figure 3 of their paper).